Check for updates

Supramolecular Pins with Ultralong Efficient Phosphorescence

Xin-Kun Ma, Wei Zhang, Zhixue Liu, Haoyang Zhang, Bing Zhang, and Yu Liu*

Constructing ultralong organic phosphorescent materials possessing a high quantum yield is challenging. Herein, assemblies of purely organic supramolecular pins composed of alkyl-bridged phenylpyridinium salts and cucurbit[8] uril (CB[8]) are reported. Different from "one host with two guests" and "head-to-tail" binding, the binding formation of supramolecular pins is "one host with one guest" and "head-to-head," which overcomes electrostatic repulsion and promotes intramolecular charge transfer. The supramolecular pin 1/CB[8] displays afterglow with high phosphorescence quantum yield (99.38%) after incorporation into a rigid matrix, which is the highest yield reported to date for phosphorescent materials. Moreover, multicolor photoluminescence can be obtained by different excitation wavelengths and ratios of host to guest. Owing to the redshift of the absorption, the supramolecular pins are applied for targeted phosphorescence imaging of mitochondria. This work will provide a reasonable supramolecular strategy to achieve redshifted and efficient phosphorescence both in the solid state and in aqueous solution.

Ultralong phosphorescent materials with long-lived emission lifetimes (>0.1 s) have applications for biological imaging[1] and information storage and encryption.[2] Purely organic phosphorescent molecules tend to have the disadvantages of a large energy gap between their singlet and triplet states (S_1 and T_1) and weak spin–orbit coupling, so various design principles have been developed to improve the efficiency of the spin–orbit coupling and to avoid quenching of the triplet excited state by suppressing triplet exciton deactivation.[3] For example, introducing heteroatom or a carbonyl group into an organic molecule has been shown to promote intersystem crossing (ISC).[4] In addition, polymer matrix,[5] crystallization,[1a,c,6] halogen binding,[4] H-aggregation,[7] and host–guest interactions[5b,8] have been used to minimize nonradiative transitions or to stabilize the triplet state energy. Cucurbiturils (CBs), which are rigid macrocyclic host synthesized by polymerization of glycoluril and formaldehyde, are ideal hosts for promoting phosphorescence under ambient conditions (in air and at room temperature). CBs bind strongly with guest molecules,[9] particularly those with a positive charge, and this binding protects against triplet

exciton quenching.[10] Research has also been directed at developing organic phosphors with redshifted emissions,[5b,11] and general strategy is to increase the extent of conjugation; however, this leads to poor water solubility and complicates synthesis. Excimers and exciplexes, which form lower energy levels because of interaction of molecules, are also a strategy to obtain redshifted emission.[12] Chi and co-workers introduced intermolecular halogen bonding to increase the ultralong phosphorescence efficiency up to 52.10%.[4c] Kim and co-workers reported a strategy to enhance phosphorescence by intermolecular interactions (halogen and hydrogen bonding).[4a] It is well known that intramolecular charge transfer (ICT) could reduce the energy gap between singlet and triplet states, Zhang and co-workers used ICT to promote phosphorescence.[13] Tian and co-workers reported multicolored luminescence based on host-enhanced ICT and host-induced restriction of intramolecular rotation. [14] Recently, our group developed synergistic enhancement strategy to achieve room-temperature phosphorescence (RTP),[2b,10,15] and we have developed multistage assembled supramolecular systems that show red and near-infrared emission by means of fluorescence resonance energy transfer and multistage assembly.[16] However, methods for using host–guest interaction to regulate ICT and to form exciplexes with efficient and tunable phosphorescence have not been reported.

In this study, we have now synthesized several novel bridged phenylpyridinium salt fluorophores with donor–acceptor moieties linked by flexible alkyl chains; compound **1** (**Scheme 1**) is a typical example. Using NMR spectroscopy, mass spectrometry (MS), transmission electron microscopy (TEM), and theoretical calculations, we analyzed the "molecular folding" binding of **1** and CB[8], and we found that **1**/CB[8] host–guest assemblies show the highest phosphorescence quantum yield reported to date for ultralong organic phosphorescence (UOP) materials. Careful comparison with reference compounds revealed the mechanistic for the efficient phosphorescence was because of three main factors: first is low rates of nonradiative decay, dispersed in a hydroxyl-rich matrix, strict encapsulation of the chromophore by CB[8] and flexible chain suppressed nonradiative decay; second, effective ICT increased the rate of ISC; finally, the formation of intramolecular halogen bond increased the rate of radiative decay from T_1 to S_0. Further, we found that supramolecular pins could be used for cell imaging, especially imaging in the mitochondrion. This supramolecular strategy

X.-K. Ma, W. Zhang, Dr. Z. Liu, H. Zhang, Dr. B. Zhang, Prof. Y. Liu
Department College of Chemistry
Nankai University
Tianjin 300071, P. R. China
E-mail: yuliu@nankai.edu.cn

The ORCID identification number(s) for the author(s) of this article can be found under https://doi.org/10.1002/adma.202007476.
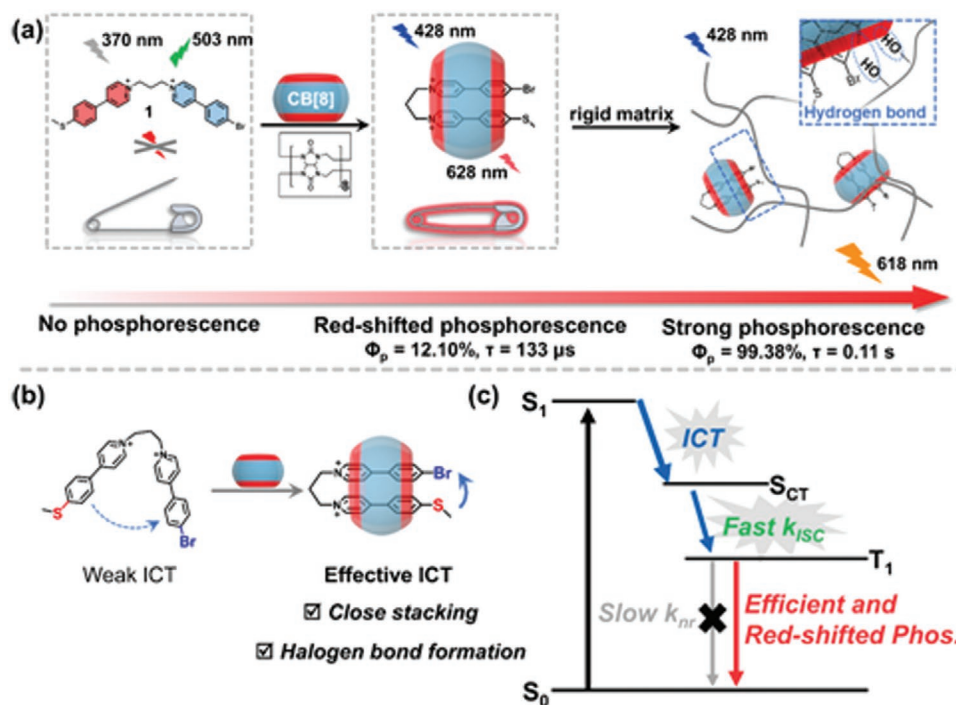
Scheme 1. a) Schematic illustration of the formation of supramolecular pin **1**/CB[8]. b) Proposed mechanism of the enhancement of ICT resulting from molecular folding. c) Possible mechanism of efficient and redshifted phosphorescence.

constitutes a unique method for realizing efficient and redshift UOP materials.

To elucidate the nature of the binding interaction between fluorophore **1** and CB[8], we began by performing UV–vis spectra titration and constructing a Job's plot based on the resulting data (Figure S1, Supporting Information). The plot indicated that the host–guest binding stoichiometry was 1:1, and the association constant (K_s) was determined to be 1.45×10^7 M^{-1} in aqueous solution (Figure S2, Supporting Information). Further evidence for the formation of a 1:1 host–guest assembly came from high-resolution MS (**Figure 1**b); in the mass spectrum, the intense peak for [**1** + CB[8] − 2Cl]$^{2+}$ (m/z 903.2344) agreed well with the calculated value (903.2418), and this result excluded the possibility of "2:2" bonding formation. Visualization of the assemblies by means of TEM (Figure S3, Supporting Information) showed that the guest molecule and the host–guest assembly were similar in size, which suggests that no supramolecular polymers or aggregates formed upon binding. In ^{1}H NMR spectroscopy (Figure 1a), the phenyl and pyridine protons of **1** shifted to higher field and the alkyl protons moved to lower field, which implied that in the assembly, the aromatic rings were enclosed in the CB[8] cavity, whereas the flexible alkyl chain was outside the cavity. Then the ^{1}H-NMR was researched more carefully, the protons of CB[8] split into two chemical shift groups, suggesting that the chemical environments of the two ports differed from each other, which provided evidence against the formation of a linear polymer resulting from head-to-tail binding. Because the chemical shift of the protons of a linear supramolecular polymer would change substantially upon dilution of the polymer,[17] we therefore measured the ^{1}H NMR spectra of **1**/CB[8] at various

concentrations. We found that the chemical shift for the protons belonging to the guest molecule had no change even when the assembly was diluted nearly 20-fold (Figure S4, Supporting Information); this result also indicates that 1:1 of **1**/CB[8] assembly was stable. Simulated structure by density functional theory provided visible image of "molecular folding" conformation (Figure 1d), bromo-substituted moiety fold back and stack with the thioether-substituted phenylpyridinium moiety, and this might result from hydrophobic effects, π–π stacking, and ion–dipole interaction. Same conclusion was also confirmed by means of 2D NMR analysis. Specifically, rotating-frame Overhauser effect spectroscopy (ROESY) of **1**/CB[8] showed strong rotating-frame nuclear Overhauser effect signals between the pyridinium groups (Figure S6a, Supporting Information), which indicates that the form of the assemblies was "head-to-head binding." The further evidence for 1:1 host–guest assembly formation was provided by diffusion-ordered NMR spectroscopy (DOSY), which showed that the diffusion coefficients (D) for **1** and **1**/CB[8] at 1×10^{-3} M were 3.28×10^{-10} and 4.97×10^{-10} m^2 s^{-1}, respectively (Figure S7, Supporting Information). According to the Stokes–Einstein relationship, D and the radius of a spherical particle in aqueous solution are inversely proportional. Comparison of the D values before and after binding indicated that **1** became smaller upon binding to CB[8], which would be reasonable if binding changed the conformation of **1** from stretched to folded. We also measured the DOSY spectra of **1**/CB[8] at various concentrations and found that D did not vary much with concentration. This lack of variation shows that the size of the assembly did not change greatly upon dilution, a result that excluded the formation not only of aggregates but also of supramolecular polymers (Figure S7e,
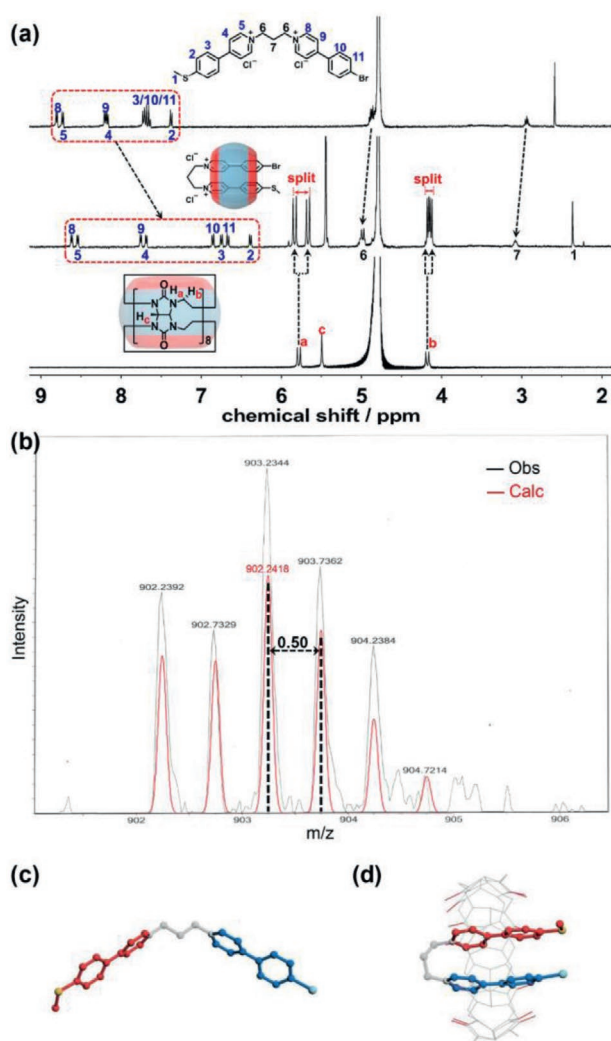
Figure 1. a) ^{1}H NMR (400 MHz, D$_2$O, 298 K) spectra of **1** (top), **1**/CB[8] (middle), and CB[8] (bottom) ([**1**] = [**1**/CB[8]] = [CB[8]] = 10.0 × 10^{-6} M). b) High-resolution electrospray ionization mass spectrum of **1**/CB[8], along with calculated spectrum. c,d) Simulated structure of **1** (left) and **1**/CB[8] (right).

Supporting Information).[16b] Furthermore, the ratio of emissions intensity around 500 and 620 nm for unbound **1** did not change with the concentration changing from 2.6 to 100 × 10^{-6} M that hint the exciplex formations were more favorable to the intramolecular process, in which phenylpyridiniums are stacked as "head-to-head" patterns (Figure S5, Supporting Information). The same result was confirmed in absorption spectra upon dilution.

The combination results of NMR, 2D NMR, TEM, MS, spectroscopic studies, and theoretical calculation indicated that the host–guest assembly between **1** and CB[8] involved "head-to-head" binding and "molecular folding." Further, we present our analysis of the optical properties of the assemblies, especially unique phosphorescent properties resulting from the effect of molecular folding. The UV–vis absorption spectrum of **1** showed peaks at around 318 and 370 nm (**Figure 2**a), which were assigned to the bromo-substituted phenylpyridinium moiety and the thioether-substituted phenylpyridinium moiety, on the

basis of comparisons to the spectra of reference compounds **1-1** and **1-2** (Figure 4). Notably, both 370 and 318 nm peaks were more redshifted relative to the corresponding peaks of the monomer (Figures S15 and S18, Supporting Information), which implies that a weak CT interaction may have occurred when the two phenylpyridine moieties were connected by the alkyl chain. Upon addition of CB[8] to **1**, the peak around 370 nm decreased in height, a new peak around 428 nm appeared, and the solution changed from almost colorless to yellow (Figure 2a). These results imply the formation of an effective CT assembly upon binding with CB[8]. Based on these observations, we speculated that the thioether-substituted phenylpyridinium moiety acted as an electron donor, and the bromo-substituted phenylpyridinium moiety acted as an electron acceptor in the CT process. The diagram in Scheme 1b shows possible CT process which suggests that the strong binding between CB[8] and **1** allowed for electronic coupling of the bromo- and thioether-substituted phenylpyridinium moieties so that electrons could effectively transfer between them.

Figure 2b shows the PL spectra of **1** in aqueous solution upon titration with CB[8]; as the concentration of CB[8] was increased, the red band (628 nm) increased to a maximum, and the green band (503 nm) became weak. In addition, during the titration with CB[8], the solution gradually changed from green to red under irradiation with 405 nm light (Figure 2b). The red band emission came from exciplexes because exciplexes typically show more redshifted emissions, larger Stokes shifts (up to 200 nm), and broader emission peaks compared with separated guest.[12] We carried out an experiment on solvent polarity-dependent PL emission, as the solvent polarity decreased, the emission around 625 nm had a significant blueshift, which further proved that CT assembly formed upon binding with CB[8] (Figure S8c, Supporting Information). Notably, the original fluorescence of the guest molecule disappeared completely upon addition of the CB[8], which implies that CT between the molecules resulted in effective conversion of the singlet electrons to the triplet state. To determine the connection between ICT and the exciplexes emission that appeared on addition of CB[8], we compared the excitation spectrum of the red band emission with the UV absorbance spectrum and found that the two spectra were almost the same (Figure S9, Supporting Information), and this confirmed that ICT proceeded from the thioether group to the bromine atom and formation of exciplexes resulted from ICT. Next, we carried out some experiments with cucurbit[7]uril (CB[7]) as a reference host, which can bind to only one of the phenylpyridinium moieties. Addition of 2.0 equiv. of CB[7] to **1** weakened the CT peak around 420 and blueshifted the fluorescence maximum emission peak by about 20 nm (Figure S10, Supporting Information), because binding of **1** with CB[7] increased the distance between the donor and acceptor moieties. We also used CB[7] to compete with CB[8] for binding with **1**, and as expected, we found that the CT absorption and the emission peak of the exciplex were quenched upon addition of CB[7] to a solution of **1**/CB[8] (Figure S11, Supporting Information). These results confirmed that CT was because of molecular folding of the guest upon binding to CB[8]. In addition, we found that the color of the solution depended on the excitation wavelength when studied the luminescence behavior of aqueous **1**/CB[8] (Figure S12a,
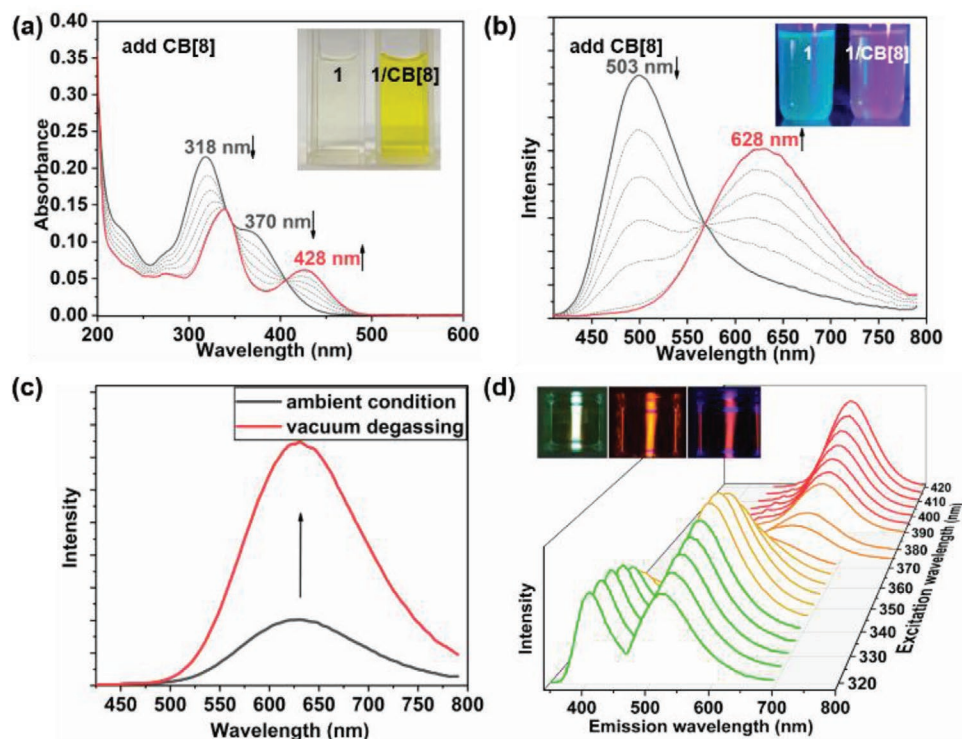
**ADVANCED
SCIENCE NEWS**

www.advancedsciencenews.com

**ADVANCED
MATERIALS**

www.advmat.de

Figure 2. Photoluminescence properties of the assemblies in aqueous solution. a) UV–vis absorption spectra of aqueous solutions of **1** (10×10^{-6} M) and CB[8] at concentrations ranging from 0 to 12×10^{-6} M under ambient conditions. Inset: photographs of solutions of **1** (1.00×10^{-3} M) and **1**/CB[8] (1.0×10^{-3} M) under ambient conditions. b) PL spectra of aqueous solutions of **1** (10×10^{-6} M) and CB[8] (excited by 428 nm) at concentrations ranging from 0 to 12×10^{-6} M under ambient conditions. Inset: photographs of solutions of **1** (1.00×10^{-3} M) and **1**/CB[8] (1.0×10^{-3} M) under 405 nm light under ambient conditions. c) PL spectra of **1**/CB[8] solution ([**1**] = [CB[8]] = 10×10^{-6} M) at room temperature under air (black) and after vacuum degassing (red). d) Emission spectra of **1**/CB[8] ([**1**] = 20×10^{-6} M, [CB[8]] = 10×10^{-6} M) in aqueous solution under ambient conditions excited with different wavelength (from 320 to 420 nm). Inset: examples of photoluminescence photographs of the **1**/CB[8] solutions under specific conditions.

Supporting Information); When the excitation wavelength gradually blueshifted to 365 nm, faint peaks were observed near 400 and 500 nm, which might be attributed to unbound guest. Owning to ITC, the absorption of unbound **1** and assembly **1**/CB[8] have significant difference (Figure 2a). When the excitation wavelength is around 420 nm, only the phosphorescence of the **1**/CB[8] can be excited, when the excitation moves to 360 nm, **1**/CB[8] and thioether-substituted phenylpyridinium moiety of unbound **1** are excited and when the excitation moves to 300 nm, only the fluorescence of the unbound **1** can be excited (Figure S12b, Supporting Information). Therefore, the solution emitted over a wide range (350–800 nm), and the emission color could be adjusted by changing the excitation wavelength and the host/guest ratio (Figure 2d).

Next, the emission lifetimes and quantum yields were measured. The lifetime at 503 nm of unbound **1** was 0.22 ns which belonged to fluorescent emission. The peak that appeared at 628 nm after addition of CB[8] had a lifetime of 133 µs (Figure S13b, Supporting Information). We obtained the following additional evidence confirming that the red band emission is phosphorescence. First, the intensity of the red band emission increased markedly upon vacuum degassing of the solution (Figure 2c); this is consistent with the fact that oxygen quenches triplet-state electrons. Second, the red band emission in solid powder and aqueous solution enhanced greatly when the temperature decreased, with the increase of

phosphorescence lifetime (Figure S14, Supporting Information), which excluded the possibility of thermally activated delayed fluorescence. Third, the time-resolved (delayed by 0.1 ms) photoluminescence spectra which were consistent with PL spectra provided another piece of evidence for phosphorescent emission (Figure S13c, Supporting Information). Upon addition of CB[8] to **1** solution, the fluorescence quantum yield is reduced from 15.24% to 0.66% and phosphorescence quantum yield is 12.10%. Without the interference of water, the phosphorescence quantum yield and lifetime of powder were increased up to 24.68% and 2.88 ms. To reduce the nonradiative transition owing to aggregation-caused quenching (ACQ) of phosphors,[10] we added the **1**/CB[8] solution with polyacrylamide (PAM), polyvinyl alcohol (PVA), and γ-cyclodextrin (γCD) (ratio of phosphors is 5%) and dripped a solution of **1**/CB[8] onto treated filter paper (see Methods section in the Supporting Information), then measured the lifetime and phosphorescence quantum yield after freeze-drying, which were found to have increased greatly (Table S3, Supporting Information). Dispersed in a hydroxyl-rich matrix, fixation of hydrogen bonds not only weakened ACQ effect but also reduced triplet state energy dissipation owing to molecular vibration.[5b] Remarkably, the phosphorescent material in the filter paper exhibited the highest phosphorescence quantum yield (99.38%) accompanied by visible afterglow (τ = 110.2 ms) (**Figure 3** and Figure S31, Supporting Information). It is worth mentioning that we
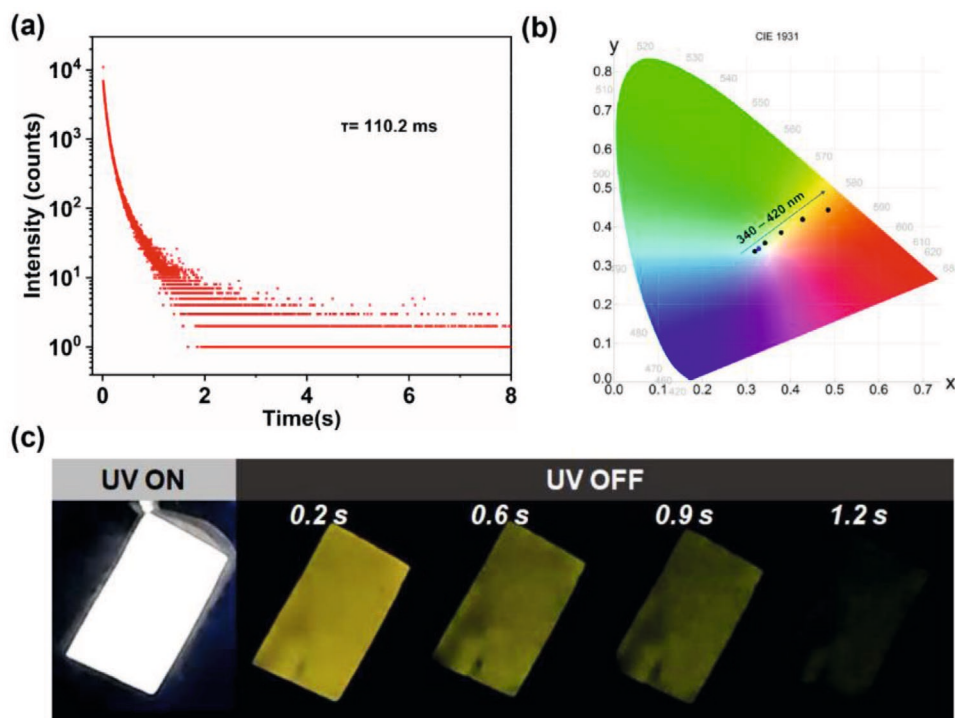
ADVANCED
SCIENCE NEWS

www.advancedsciencenews.com

ADVANCED
MATERIALS

www.advmat.de

Figure 3. Photoluminescence properties of the assemblies in solid state. a) Time-resolved photoluminescence decay **1**/CB[8] embedded in filter paper at 620 nm under ambient conditions. b) CIE 1931 chromaticity diagram of filter paper embedded with assemblies **1**/CB[8] with different exciting wavelength (from 320 to 420 nm, blue dot is 365 nm). c) Afterglow images of filter paper embedded with assemblies **1**/CB[8] under 365 nm with the excitation source on and off.

have eliminated the interference of eliminating blank filter paper (Figure S32, Supporting Information). The film after dispersion exhibited sensitivity to excitation wavelength, which is similar to solution state, and displayed color transition from white to orange (Figure 3b).

It is well-known that bright, long-lived phosphorescence requires fast ISC from $S_1 \rightarrow T_n$ and slow nonradiative decay from T_1 to S_0. According to El-Sayed's rules, the introduction of heteroatoms (e.g., bromine and sulfur) will increase the rate of ISC because $^1(\pi, \pi^\star) \rightarrow {}^3(n, \pi^\star)$ and $^3(\pi, \pi^\star) \rightarrow {}^1(n, \pi^\star)$ are faster than $^1(\pi, \pi^\star) \rightarrow {}^3(\pi, \pi^\star)$ or $^1(n, \pi^\star) \rightarrow {}^3(n, \pi^\star)$.[18] Br and S with lone-pair electrons provide the luminescent core with dominant (n, $\pi^\star$) characteristic. However, introduction of lone-pair electrons did not seem to be the only reason for effective phosphorescence generation. For use as reference compounds, we synthesized **1-1** and **1-2**, which have lone-pair electrons but no bridges. Upon addition of CB[8], both **1-1** and **1-2** showed similar fluorescence quenching (**Figure 4** and Figures S15 and S18, Supporting Information). Moreover, the decrease in the emission intensity of guests was not accompanied by activation of an effective phosphorescence. Low k_{ISC} (ISC rate) might result from loose binding and inefficient intermolecular charge transfer (Table S2, Supporting Information). When CB[8] was gradually added to solutions containing equal concentrations of **1-1** and **1-2**, both the UV–vis absorption and emission spectra of the resulting solution corresponded roughly to the spectra that would be expected from simple addition of the spectra of **1-1**/CB[8] and **1-2**/CB[8] (Figure S21, Supporting Information) and did not show peak around 628 nm after binding with CB[8],

which excluded the possibility of assembly into a linear supramolecular polymer by means of "head-to-tail" binding.

To further study the synergy between molecular folding and lone-pair electrons, we synthesized **5**, which has two thioether-substituted phenylpyridinium moieties. The emission belonging to guest was completely quenched upon addition of CB[8], as was the case for **1** (Figure 4 and Figure S22b, Supporting Information). However, no new emission belonging to exciplex appeared upon addition of CB[8]. The high $\emptyset_{ISC}$ (quantum efficiency of ISC from S_1 to T_n states) of **5**/CB[8] was derived from the proximity of lone-pair electrons as a result of molecular folding which seemed to be inconsistent with the fact that effective phosphorescence emission was not observed. We hypothesized that efficient transfer of electrons from the S_1 state to the T_n state and the fact that no new peaks appeared was owing to k_p being much slower than k_{nr} (which are the rates of radiative and nonradiative decay of T_1 to S_0). To test this hypothesis, we froze a solution of **5**/CB[8] in liquid nitrogen and irradiated it with 400 nm light; not surprisingly, we observed a strong orange-red afterglow under these conditions (Figure S22d, Supporting Information). The activation of phosphorescence was because of inhibition of the nonradiative transition at the low temperature. In contrast, when a solution of unbound **5** was frozen in liquid nitrogen, only green fluorescence was observed (Figure S22c, Supporting Information). The difference with **5**/CB[8] is that **1**/CB[8] formed halogen bond between Br and S after folding. In other words, the formation of intramolecular halogen bond between moieties of guest after folding facilitated ISC. To explore this effect, we
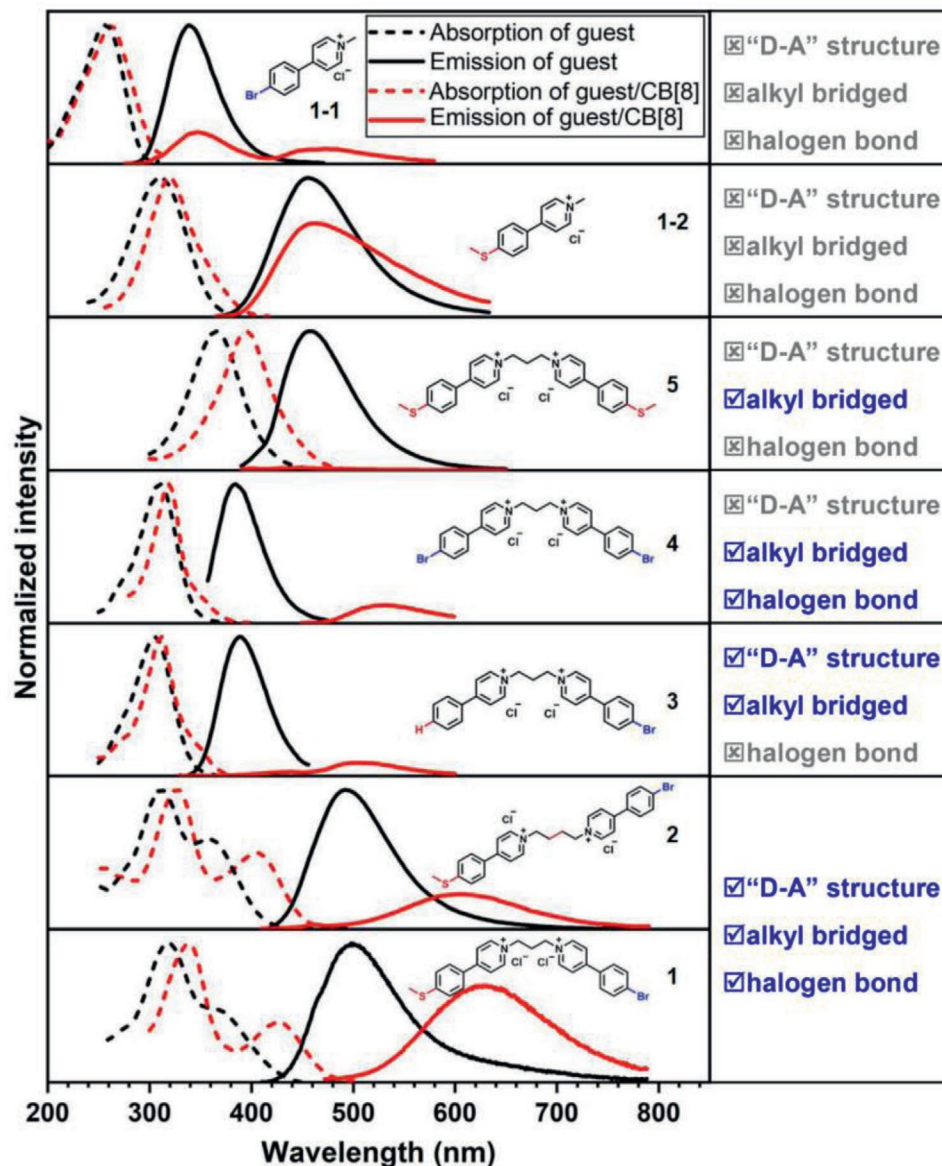
ADVANCED
SCIENCE NEWS

www.advancedsciencenews.com

ADVANCED
MATERIALS

www.advmat.de

Figure 4. Optical properties of **1** and reference compounds. UV–vis absorption spectra of guest molecules and guest/CB[8] complexes and PL spectra of guest molecules and guest/CB[8] complexes.

evaluated the CB[8] binding behavior of reference compound **4**, which could form halogen bond and possessed lone-pair electrons. Upon addition of 1 equiv of CB[8] to **4** solution, a phosphorescence peak around 531 nm appeared and gradually increased in intensity, and this process was accompanied by almost complete quenching of the peak for **4** around 385 nm (Figure S23b, Supporting Information, and Figure 4). The halogen bond between the two bromine atoms that formed after the addition of CB[8] further enhanced k_{ISC}. Comparing with **1** and **1**/CB[8], the phosphorescence quantum yield of the **4**/CB[8] is much lower than the fluorescence quantum yield of the unbound **4** (Tables S1 and S2, Supporting Information). We also tested reference compound **3**, which has donor–acceptor structure but cannot form a halogen bond. Upon addition of CB[8] to **3**, a weak CT absorption peak and a phosphorescence peak were generated, and the emission peak for unbound **3**

was not completely quenched, which implies that electronic coupling via the halogen bond promoted ISC (Figure S24, Supporting Information, and Figure 4). Comprehensive consideration from the **3**/CB[8], **4**/CB[8], and **5**/CB[8], we concluded that it was synergistic enhancement of halogen bond and CT which could activate RTP by accelerating k_{ISC}, and this synergy is inseparable from "molecular folding."

The other requirement to achieve long-lived and highly efficient RTP is to reduce nonradiative decay rates from T_1 to S_0, that is, slow k_{nr}.[19] In our system, the flexible alkyl chain plays an important role in the molecular folding that occurred upon binding to CB[8] and was used to promote intramolecular interactions—that is, folding allowed for $\pi-\pi$ stacking of the aryl rings, intramolecular halogen bonding, and ICT, which were important factors leading to efficient phosphorescence. **2** was synthesized to find the effect of flexible chain length on
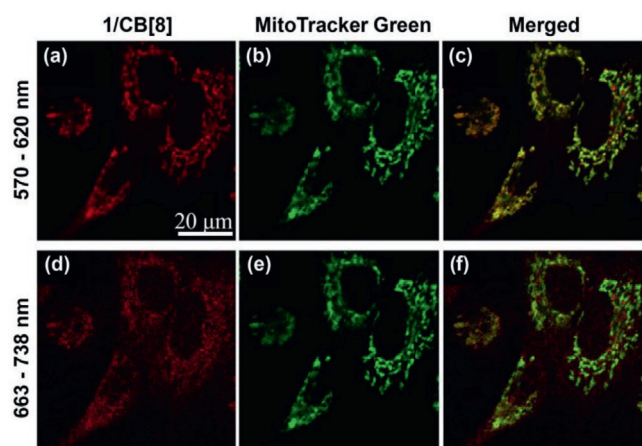
**ADVANCED
SCIENCE NEWS**

www.advancedsciencenews.com

**ADVANCED
MATERIALS**

www.advmat.de

Figure 5. Confocal microscopy images. A549 cells incubated with **1**/CB[8] ([**1**] = [CB[8]] = 50×10^{-6} M). MitoTracker Green (green) was used to stain the mitochondria. a) Phosphorescence image of **1**/CB[8] (408 nm laser/570–620 nm filter). b,e) Fluorescence image of MitoTracker Green. c) Merged image of (a) and (b). d) Phosphorescence image with 408 nm laser/663–738 nm filter. f) Merged image of (d) and (e).

phosphorescence. Spectrum titration was performed to give association constant (K_s) of **2**/CB[8] (1.37×10^7 M^{-1}), which was similar to K_s of **1**/CB[8] (1.45×10^7 M^{-1}), indicating that the length of the alkyl chain will not affect the binding (Figure S25d, Supporting Information). The length of the alkyl chain might affect the degree of π–π stacking. In Figure 4, the absorption and emission of **2** and **2**/CB[8] are both blueshifted compared with **1** and **1**/CB[8]. **2** bearing longer alkyl chain formed a loose structure after binding with CB[8], which may lead to phosphorescence quenching. In addition, CB[8] as a macrocycle host capsules the guest to protect from reaggregation and promote restriction of intramolecular rotation, which prevents energy dissipation. Embedding and dispersing the assemblies into a rigid matrix can further reduce nonradiative transition caused by molecular vibrations and interactions with water and oxygen. For example, filter paper, the main component of which is cellulose, and which has many hydroxyl groups, can form hydrogen bond with CBs and then restrict the movement of molecules (Scheme 1). Synergistic suppressions of alkyl chain, CB[8], and rigid matrix make long-lived phosphorescence display.

Benefiting from redshift of the absorption peak to the visible-light zone by ICT, supramolecular assemblies can be applied in cell imaging. In **Figure 5**, the confocal laser scanning microscopy of A549 cells with incubation of **1**/CB[8] suggested that assemblies could be easily internalized into the cell and displayed an effective red phosphorescence, which showed a good colocalization with the MitoTracker Green (mitochondria marker).

In summary, we prepared a series of supramolecular pins composed of CB[8] and alkyl-bridged bis(phenylpyridinium) compounds. NMR, 2D NMR, TEM, MS, spectroscopic studies, and theoretical calculation revealed that the alkyl-bridged phenylpyridinium compounds adopted folded structures upon binding to CB[8]. We confirmed that the high phosphorescence quantum yield and long lifetime of **1**/CB[8] were mainly owing not to trapping of **1** but to intramolecular interactions between **1** and CB[8]; that is, the efficient ISC crossing exhibited by this assembly was attributed mainly to π–π stacking of

the aryl rings, proximity of lone-pair electrons, intramolecular halogen bond formation, and ICT, which is induced by folding of the guest molecule. Furthermore, the rigidity of CB[8] and the motion restrictions imposed by the alkyl chain, the halogen bond, and the rigid matrix all reduced the loss of triplet energy. In addition, supramolecular pins were applied for targeted phosphorescent imaging of mitochondria. The supramolecular assembly strategy described herein has potential utility for facilitating the development of purely organic phosphors for biological imaging and anti-counterfeiting applications.

Conflict of Interest

The authors declare no conflict of interest.

Data Availability Statement

The data that support the findings of this study are available from the corresponding author upon reasonable request.

[1] a) J. Yang, X. Zhen, B. Wang, X. Gao, Z. Ren, J. Wang, Y. Xie, J. Li, Q. Peng, K. Pu, Z. Li, *Nat. Commun.* **2018**, *9*, 840; b) L. M. Hirvonen, M. Fisher-Levine, K. Suhling, A. Nomerotski, *Rev. Sci. Instrum.* **2017**, *88*, 013104; c) S. M. A. Fateminia, Z. Mao, S. Xu, Z. Yang, Z. Chi, B. Liu, *Angew. Chem., Int. Ed.* **2017**, *56*, 12160.

[2] a) Y. Su, S. Z. F. Phua, Y. Li, X. Zhou, D. Jana, G. Liu, W. Q. Lim, W. K. Ong, C. Yang, Y. Zhao, *Sci. Adv.* **2018**, *4*, eaas9732; b) Z.-Y. Zhang, Y. Liu, *Chem. Sci.* **2019**, *10*, 7773.

[3] a) Y. Tao, R. Chen, H. Li, J. Yuan, Y. Wan, H. Jiang, C. Chen, Y. Si, C. Zheng, B. Yang, G. Xing, W. Huang, *Adv. Mater.* **2018**, *30*, 1803856; b) Kenry, C. C. , B. Liu, *Nat. Commun.* **2019**, *10*, 2111; c) W. Zhao, Z. He, B. Z. Tang, *Nat. Rev. Mater.* **2020**, *5*, 869.

[4] a) O. Bolton, K. Lee, H. J. Kim, K. Y. Lin, J. Kim, *Nat. Chem.* **2011**, *3*, 205; b) Z. Yang, C. Xu, W. Li, Z. Mao, X. Ge, Q. Huang, H. Deng,

J. Zhao, F. L. Gu, Y. Zhang, Z. Chi, *Angew. Chem., Int. Ed.* **2020**, *59*, 17451.

[5] a) H. Wang, H. Shi, W. Ye, X. Yao, Q. Wang, C. Dong, W. Jia, H. Ma, S. Cai, K. Huang, L. Fu, Y. Zhang, J. Zhi, L. Gu, Y. Zhao, Z. An, W. Huang, *Angew. Chem., Int. Ed.* **2019**, *58*, 18776; b) Y. Su, Y. Zhang, Z. Wang, W. Gao, P. Jia, D. Zhang, C. Yang, Y. Li, Y. Zhao, *Angew. Chem., Int. Ed.* **2020**, *59*, 9967. c) M. S. Kwon, D. Lee, S. Seo, J. Jung, J. Kim, *Angew. Chem., Int. Ed.* **2014**, *53*, 11177.

[6] Z. He, W. Zhao, J. W. Y. Lam, Q. Peng, H. Ma, G. Liang, Z. Shuai, B. Z. Tang, *Nat. Commun.* **2017**, *8*, 416.

[7] Z. An, C. Zheng, Y. Tao, R. Chen, H. Shi, T. Chen, Z. Wang, H. Li, R. Deng, X. Liu, W. Huang, *Nat. Mater.* **2015**, *14*, 685.

[8] a) L. Xu, L. Zou, H. Chen, X. Ma, *Dyes Pigm.* **2017**, *142*, 300; b) Y. Gong, H. Chen, X. Ma, H. Tian, *ChemPhysChem* **2016**, *17*, 1934.

[9] E. Pazos, P. Novo, C. Peinador, A. E. Kaifer, M. D. Garcia, *Angew. Chem., Int. Ed.* **2019**, *58*, 403.

[10] Z. Y. Zhang, W. W. Xu, W. S. Xu, J. Niu, X. H. Sun, Y. Liu, *Angew. Chem., Int. Ed.* **2020**, *59*, 18748.

[11] Y. Lei, W. Dai, J. Guan, S. Guo, F. Ren, Y. Zhou, J. Shi, B. Tong, Z. Cai, J. Zheng, Y. Dong, *Angew. Chem., Int. Ed.* **2020**, *59*, 16054.

[12] S.-H. Li, X. Xu, Y. Zhou, Q. Zhao, Y. Liu, *Org. Lett.* **2017**, *19*, 6650.

[13] X. Chen, C. Xu, T. Wang, C. Zhou, J. Du, Z. Wang, H. Xu, T. Xie, G. Bi, J. Jiang, X. Zhang, J. N. Demas, C. O. Trindle, Y. Luo, G. Zhang, *Angew. Chem., Int. Ed.* **2016**, *55*, 9872.

[14] Q. W. Zhang, D. Li, X. Li, P. B. White, J. Mecinovic, X. Ma, H. Agren, R. J. M. Nolte, H. Tian, *J. Am. Chem. Soc.* **2016**, *138*, 13541.

[15] a) J.-J. Li, H.-Y. Zhang, Y. Zhang, W.-L. Zhou, Y. Liu, *Adv. Opt. Mater.* **2019**, *7*, 1900589; b) Z.-Y. Zhang, Y. Chen, Y. Liu, *Angew. Chem., Int. Ed.* **2019**, *58*, 6028.

[16] a) X.-M. Chen, Y. Chen, Q. Yu, B.-H. Gu, Y. Liu, *Angew. Chem., Int. Ed.* **2018**, *57*, 12519; b) X. Wu, Y. Chen, Q. Yu, F.-Q. Li, Y. Liu, *Chem. Commun.* **2019**, *55*, 4343.

[17] L. Chen, Y. Chen, H.-G. Fu, Y. Liu, *Adv. Sci.* **2020**, *7*, 2000803.

[18] a) Y. Xiong, Z. Zhao, W. Zhao, H. Ma, Q. Peng, Z. He, X. Zhang, Y. Chen, X. He, J. W. Y. Lam, B. Z. Tang, *Angew. Chem., Int. Ed.* **2018**, *57*, 7997; b) Z. Yang, Z. Mao, X. Zhang, D. Ou, Y. Mu, Y. Zhang, C. Zhao, S. Liu, Z. Chi, J. Xu, Y. C. Wu, P. Y. Lu, A. Lien, M. R. Bryce, *Angew. Chem., Int. Ed.* **2016**, *55*, 2181.

[19] H. Ma, Q. Peng, Z. An, W. Huang, Z. Shuai, *J. Am. Chem. Soc.* **2019**, *141*, 1010.